

07.2

InSb/GaAs heterostructures for magnetic field sensors

© M.A. Sukhanov¹, D.Yu. Protasov^{1,2}, A.K. Bakarov¹, A.A. Makeeva¹, I.D. Loshkarev¹, K.S. Zhuravlev¹

¹Rzhanov Institute of Semiconductor Physics, Siberian Branch, Russian Academy of Sciences, Novosibirsk, Russia

²Novosibirsk State Technical University, Novosibirsk, Russia

E-mail: msukhanov@isp.nsc.ru

Received May 4, 2023

Revised May 4, 2023

Accepted September 5, 2023

Structural defects and transport properties have been studied in InSb layers grown on GaAs substrates by molecular beam epitaxy. The composition of the buffer layer which ensures the lowest defect density and electron mobility of about $39\,000\text{ cm}^2/(\text{V}\cdot\text{s})$ at room temperature in undoped InSb layers $0.5\mu\text{m}$ thick was determined. A Hall sensor based on *n*-type InSb layers with a high room-temperature sensitivity ($\sim 27\text{ V}/(\text{A}\cdot\text{T})$) was created.

Keywords: molecular beam epitaxy, InSb layers on GaAs, Hall sensor, heteroepitaxy.

DOI: 10.61011/TPL.2023.10.57062.19617

Hall sensors are widely used for measuring magnetic field characteristics in many fields of science and technology. The most important parameters of the sensors are sensitivity to magnetic field (S) defined as $S = U_H/B$ (where U_H is the Hall voltage, B is the magnetic induction), and also temperature stability of the sensitivity. The sensor sensitivity is determined by different structure parameters depending on the operating mode. In the mode of direct current passing through the structure

$$S_I = \frac{I}{e n d}, \quad (1)$$

where I is the direct current, n is the electron concentration in the structure's active layer, d is the layer thickness, e is the electron charge; in the mode of applied DC voltage, $S_U \propto \mu$ (here μ is the charge carrier mobility); in the mode of constant electric field power, $S_p \propto \sqrt{\mu/n d}$. Hence, in the first case thin layers of narrow-bandgap semiconductors are used to enhance the Hall sensor sensitivity, but high resistance of the sensor hinders fabrication of ohmic contacts. In the second mode, materials with high charge carrier mobility are preferable. In the third case, the sensors should be better fabricated by using thin layers of materials with high mobility and low concentration of the charge carriers.

InSb is a narrow-bandgap semiconductor possessing high mobility $\mu \geq 60\,000\text{ cm}^2/(\text{V}\cdot\text{s})$ and intrinsic electron concentration of $2 \cdot 10^{16}\text{ cm}^{-3}$ at $T = 300\text{ K}$ [1]. When InSb is used as an active layer, the temperature variation by one degree results in relative variation in the intrinsic concentration by 2.2%; semiconductors with wider band gaps exhibit a greater intrinsic concentration variation in percentage (for instance, for Si it is 8.3% per degree). Thus, due to high mobility and weak temperature dependence of the intrinsic concentration of electrons, InSb are being widely used in producing magnetic field sensors. Since non-conductive InAs substrates are unavailable, the InSb layers intended for fabricating the Hall sensors are being grown on semi-insulating GaAs substrates or high-resistance Si substrates.

The lattice mismatch between InSb and GaAs ($\sim 14\%$), as well as between InSb and Si ($\sim 19\%$), generates on the heteroboundary dislocations, stacking faults and twins which reduce the charge carrier mobility and deteriorate the device characteristics. The electron mobility in InSb layers grown on GaAs without additional buffer layers increases with increasing layer thickness due to a decrease in the structural defects density and equals $\sim 60\,000\text{ cm}^2/(\text{V}\cdot\text{s})$ at the thickness of $2\mu\text{m}$ and temperature of 300 K [1]. Introduction of buffer layers between the GaAs substrate and InSb layer reduces the defects density and increases the electron mobility [2], which allows one to reduce the InSb layer thickness without reducing the electron mobility and, hence, to improve the Hall sensor sensitivity. To enhance the temperature stability of the sensitivity, the InSb layers are being doped with donors.

According to literature data, the InSb layers for Hall sensors are being grown by molecular beam epitaxy (MBE) and flash evaporation; the latter is used most often [3–7]. MBE-grown InSb layers exhibit a lower density of structural defects [4] than layers grown by flash evaporation; this allows obtaining a higher electron mobility and higher sensitivity to magnetic field.

The goal of this study was to search for a better buffer layer structure and conditions for MBE growth of InSb heterostructures intended for producing highly sensitive temperature-stable Hall sensors.

The InSb-based heterostructures were grown at the MBE setup Riber Compact 21 T equipped with a valved source of antimony and sources of aluminum, indium and silicon. The growth process was controlled by the method of fast-electron diffraction (FED). The growth rates and layer compositions were determined via oscillations of the FED patterns' specular beam. As per data obtained in [8], the GaAs substrate surfaces of all the samples were kept in the Sb flux at the stage of removing the oxide; after that, the AlSb layer 20 nm thick was grown. As shown by the FED pattern, the three-dimensional growth mode was observed

I		II		III		IV	
InSb	0.5 μm	InSb	0.5 μm	InSb	0.5 μm	InSb	0.5 μm
In _{0.75} Al _{0.25} Sb	1 μm	In _{0.85} Al _{0.15} Sb	0.2 μm	InSb/In _{0.85} Al _{0.15} Sb SL (2.5/2.5 nm) \times 10		In _{0.85} Al _{0.15} Sb	0.3 μm
AlSb	20 nm	In _{0.75} Al _{0.25} Sb	0.8 μm	In _{0.85} Al _{0.15} Sb	0.2 μm	In _{0.75} Al _{0.25} Sb SL (2.5/2.5 nm) \times 10	
		AlSb	20 nm	In _{0.75} Al _{0.25} Sb	0.8 μm	In _{0.75} Al _{0.25} Sb	1.2 μm
				AlSb	20 nm	AlSb	20 nm

Figure 1. Compositions of buffer layers.

during growing the initial AlSb monolayers; at the end of the AlSb layer growth, transition to the two-dimensional growth mode occurred. After that, the buffer layer and InSb layer 0.5 μm thick were grown. The InSb and InAlSb layers of all the structures were grown under the conditions of the surface enrichment with antimony, which was controlled via the existence of surface reconstruction (1×3).

Fig. 1 schematically illustrates heterostructures with different buffer structures (Samples I–IV). The material most suitable for creating the buffer layer is In_{1-x}Al_xSb because of its lower lattice mismatch with InSb ($\sim 0.7\%$ at $x = 0.15$) and wider band gap ($E_g \approx 0.43$ eV at $T = 300$ K) [9]. As the aluminum fraction decreases, the mismatch with InSb decreases and intrinsic conductivity increases; this restricts the minimal content of aluminum. The use of strained superlattices (SL) in the buffer layers leads to a reduction in the density of threading dislocations [2,10]; therefore, one of the samples was fabricated by using a short-period strained InSb/InAlSb superlattice. To find out the best buffer layer, surface morphology of the grown heterostructures was studied by atomic force microscopy (AFM). Structural perfection of the layers was assessed by high-resolution X-ray diffractometry using the CuK $_{\alpha 1}$ X-rays and Ge (004) monochromator. The electron concentration and mobility were determined by the Van-der-Pauw method at $T = 300$ K and $B = 0.2$ T. After the best buffer layer was found out, based on it there was grown a heterostructure involving an aluminum-doped InSb layer having the thickness of 0.5 μm and donor concentration of $4.5 \cdot 10^{17}$ cm $^{-3}$, namely, Sample V. To calibrate the source of silicon, doped InSb layers 5 μm thick were grown on GaAs, and the concentration was measured by the Van-der-Pauw method at $T = 77$ K. The magnetic field sensor was fabricated based on Sample V by the methods of photolithography and liquid etching with sputtering metallic (Ti/Au) contacts.

Fig. 2, *a* presents an AFM image of the Sample I surface; circles mark the regions containing typical defects. Surfaces of all the samples exhibited defects of three types: defects of the *A* type are non-monoatomic steps, defects *B* are hills, defects *C* are truncated pyramids. All the mentioned defects are typical of the InSb layers on GaAs. Defects of the *A* type arise due to formation of twin defects [11]. Defects *B* arise because of growing around screw dislocations, defects *C* result from formation of stacking faults crossing the (001) surface in the $[\bar{1}10]$ and $[110]$ directions [12].

Fig. 2, *b* demonstrates for Sample IV a distribution pattern of the diffracted X-rays intensity in the reciprocal space near the InSb (004) node. Three broadened reflexes correspond to three heterostructure layers. The frame-of-reference origin was assumed to be located at the X-ray maximum corresponding to the InSb layer. The node extension along the *OY* axis is connected with orientational distortions of the layer lattice mainly due to the presence of mismatch dislocations. The node extension along the *OZ* axis is caused by the lattice parameter distortion due to the presence of defects of various types. Structural perfection of the InSb layers was assessed via the InSb (004) node FWHM along *OZ* (designated as dq_z in Fig. 2, *b*). The minimal dq_z value was observed for Sample IV.

The Table presents the densities of the *A* and *B* defects, FWHM of the InSb (004) node, and electron mobility and concentration in InSb layers. The Table shows that, as the density of the *A* and *B* defects decreases, FWHM decreases and electron mobility increases. Defects *C* are non-uniformly distributed over the sample surfaces, and their influence on the mobility is weaker because of a lower density. As shown by the Table data, the electron mobility almost identically increases due to a decrease in the structural defect density in the case of using two superlattices (Sample III) and in the case of increasing the InAlSb layer thickness by 0.5 μm (Sample IV). The effect of structural defects on the electron

Charge carrier parameters and defect density of the grown samples

Sample	n, cm^{-3}	$\mu, \text{cm}^2/(\text{V} \cdot \text{s})$	Density of defects A, cm^{-1}	Density of defects B, cm^{-2}	FWHM (dq_z), \AA^{-1}
I	$2.06 \cdot 10^{16}$	31748	856	10^7	0.00251
II	$2.04 \cdot 10^{16}$	34518	692	$7.5 \cdot 10^6$	0.00228
III	$1.97 \cdot 10^{16}$	37967	636	$7.1 \cdot 10^6$	0.00226
IV	$2.06 \cdot 10^{16}$	38714	521	$4.4 \cdot 10^6$	0.00205
V	$4.5 \cdot 10^{17}$	16300			—

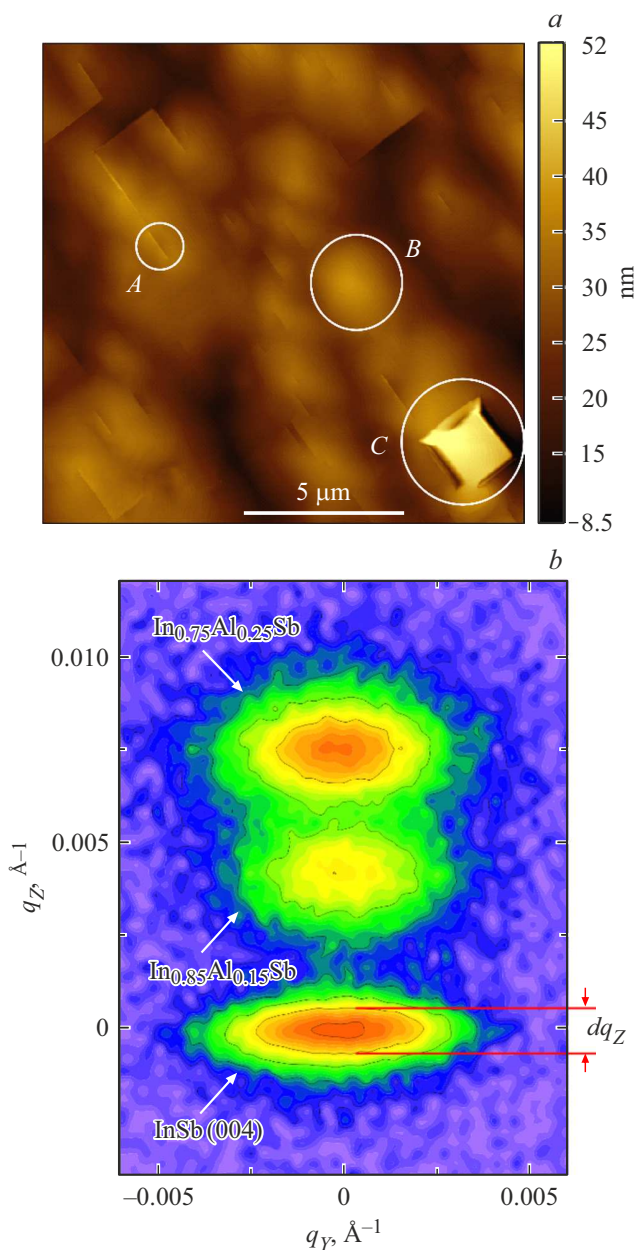


Figure 2. *a* — AFM image of the Sample I surface. White circles mark the typical observed defects. *b* — Sample IV reciprocal space pattern. Horizontal lines indicate FWHM of node (004) of the InSb active layer.

mobility will be discussed in more detail in our next paper. Notice that the electron mobility in the InSb layer having the thickness of $0.5 \mu\text{m}$ and electron concentration of $\sim 4.5 \cdot 10^{17} \text{cm}^{-3}$, which is used in fabricating the sensor, is higher than that in the flash-evaporated InSb layers with the thickness of $1.1 \mu\text{m}$ and concentration of $4 \cdot 10^{17} \text{cm}^{-3}$ [4]; this indicates high structural perfection of the MBE-grown InSb layers. The data obtained enabled determining the buffer layer structure (Sample IV) ensuring the best structural and transport characteristics of the InSb layers.

Sensitivity of the Hall sensor was measured in the DC mode at $I = 1 \text{mA}$ in the temperature range $T = 77\text{--}330 \text{K}$. Fig. 3 presents the temperature dependence of the sensor sensitivity obtained in this study, and also the same dependences taken from [4,6]. The sensitivity is normalized to the current. The sensitivity reduction with increasing temperature is associated with an increase in the intrinsic electron concentration in the InSb layer. As Fig. 3 shows, the sensitivity of the sensor obtained in this work is higher than that in [4,6], which is connected with a smaller layer thickness and difference in doping degrees. The ratio between the sensitivity of the sensor presented in this work and those of sensors from [4–7] is well describable by formula (1); the formula predicts a higher sensitivity for the sensor based on undoped InSb [3]. Reduction in the sensor sensitivity may be associated with high conductivity of the InSb buffer layer. Typically, reduction in the InSb layer thickness increases its resistance due to the electron mobility decrease caused by a growth of the defect density near the buffer. The increase in resistance makes it necessary to increase the voltage needed for maintaining the direct current flowing through the sensor, which shrinks the sensor application range [7]. A similar situation is observed also in other operating modes of the sensor when deterioration of the structures quality has to be compensated by enhancing the energy consumption, which is unacceptable in many applications.

Thus, in this work optimization of the buffer layer structure was performed, which resulted in an efficient reduction in the structural defect density and increase in the electron mobility and conductivity of the InSb active layer. This made it possible to improve the sensitivity of

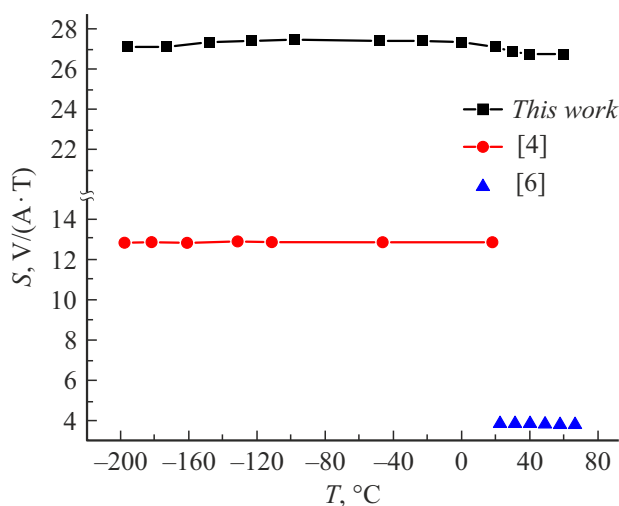


Figure 3. Temperature dependences of sensitivity of the InSb-based Hall sensors obtained in this work and works [4,6].

the magnetic field sensor without deteriorating its operating mode.

Financial support

The study was accomplished in the framework of State Assignment for ISP SB RAS (code FWGW-2022-0005).

Conflict of interests

The authors declare that they have no conflict of interests.

References

- [1] T. Zhang, S.K. Clowes, M. Debnath, A. Bennett, C. Roberts, J.J. Harris, R.A. Stradling, L.F. Cohena, T. Lyford, P.F. Fewster, *Appl. Phys. Lett.*, **84** (22), 4463 (2004). DOI: 10.1063/1.1748850
- [2] X. Zhao, Y. Zhang, M. Guan, L. Cui, B. Wang, Z. Zhu, Y. Zeng, *J. Cryst. Growth*, **470**, 1 (2017). DOI: 10.1016/j.jcrysgro.2017.03.051
- [3] O. Kazakova, J.C. Gallop, P. See, D. Cox, G.K. Perkins, J.D. Moore, L.F. Cohen, *IEEE Trans. Magn.*, **45** (10), 4499 (2009). DOI: 10.1109/TMAG.2009.2025513
- [4] M. Oszwaldowski, T. Berus, *Thin Solid Films*, **515** (4), 2692 (2006). DOI: 10.1016/j.tsf.2006.07.023
- [5] T. Berus, M. Oszwaldowski, J. Grabowski, *Sensors Actuators A*, **116** (1), 75 (2004). DOI: j.sna.2004.03.029
- [6] S. El-Ahmar, M. Przychodnia, J. Jankowski, R. Prokopowicz, M. Ziemia, M.J. Szary, W. Reddig, J. Jagiełło, A. Dobrowolski, T. Ciuk, *Sensors*, **22** (14), 5258 (2022). DOI: 10.3390/s22145258
- [7] J. Jankowski, S. El-Ahmar, M. Oszwaldowski, *Sensors*, **11** (1), 876 (2011). DOI: 10.3390/s110100876
- [8] A.N. Semenov, B.Ya. Meltser, V.A. Solov'ev, T.A. Komissarova, A.A. Sitnikova, D.A. Kirylenko, A.M. Nadtochy, T.V. Popova, P.S. Kop'ev, S.V. Ivanov, *Semiconductors*, **45** (10), 1327 (2011). DOI: 10.1134/S1063782611100150
- [9] G. Chen, W. Sun, Y. Lv, *Infrared Phys. Technol.*, **81**, 262 (2017). DOI: 10.1016/j.infrared.2017.01.014
- [10] A.E. Blakeslee, *MRS Online Proceedings Library*, **148**, 217 (1989). DOI: 10.1557/PROC-148-217
- [11] T.D. Mishima, J.C. Keay, N. Goel, M.A. Ball, S.J. Chung, M.B. Johnson, M.B. Santos, *Physica E*, **20** (3-4), 260 (2004). DOI: 10.1016/j.physe.2003.08.014
- [12] M.A. Ball, J.C. Keay, S.J. Chung, M.B. Santos, M.B. Johnson, *Appl. Phys. Lett.*, **80** (12), 2138 (2002). DOI: 10.1063/1.1463206

Translated by Solonitsyna Anna